The Role of Monomers and Dimers in the Reduction of Ruthenium(II) Complexes of Redox-Active Tetraazatetrapyridopentacene Ligand

Norma R. de Tacconi,[†] Rungano Chitakunye,[†] Frederick M. MacDonnell,*[,†] and Reynaldo O. Lezna[‡]

Department of Chemistry and Biochemistry, The University of Texas at Arlington, Arlington, Texas 76019-0065, and INIFTA-CONICET, CC.16, Suc. 4, La Plata B1906ZAA, Argentina

Received: August 31, 2007; In Final Form: October 23, 2007

A combination of electrochemistry, spectroelectrochemistry, and ^{1}H NMR has been used to study the reduction and solution speciation in acetonitrile of two mononuclear Ru complexes containing the redox-active 9,11,-20,22-tetraazatetrapyrido [3,2-*a*:2′,3′-*c*:3″,2″-l:2‴,3‴-*n*]pentacene (tatpp) ligand. These complexes, $[(bpy)_2Ru(tatpp)][PF_6]_2$ (**1**$[PF_6]_2$), and $[(phen)_2Ru(tatpp)][PF_6]_2$ (**2**$[PF_6]_2$) (where bpy is 2,2′-bipyridine and phen is 1,10-phenanthroline), form $\pi-\pi$ stacked dimers (e.g., π-$\{\mathbf{1}\}_2^{4+}$ and π-$\{\mathbf{2}\}_2^{4+}$) in solution as determined by ^{1}H NMR studies in an extended concentration range (90 − 5000 μM) as well as via simulation of the electrochemical data. The dimerization constant for $\mathbf{1}^{2+}$ in acetonitrile is 2×10^4 M^{-1} as determined from the NMR data. Slightly higher dimerization constants (8×10^4 M^{-1}) were obtained via simulation of the electrochemical data and are attributed to the presence of the supporting eletrolyte. Electrochemical and spectroelectrochemical data show that the $\pi-\pi$ stacked dimers are electroreduced in two consecutive steps at −0.31 and −0.47 V vs Ag/AgCl, which is assigned to the uptake of one electron by each tatpp ligand in π-$\{\mathbf{1}\}_2^{4+}$ to give first π-$\{\mathbf{1}\}_2^{3+}$and then π-$\{\mathbf{1}\}_2^{2+}$. At potentials negative of −0.6 V, the electrochemical data reveal two different reaction pathways depending on the complex concentration in solution. At low concentrations ($\leq$20 μM), the next electroreduction occurs on a monomeric species (e.g., $[(bpy)_2Ru(tatpp)]^{+/0}$) showing that the doubly reduced $\pi-\pi$ dimer ($\pi-\{\mathbf{1}\}_2^{2+}$ and $\pi-\{\mathbf{2}\}_2^{2+}$) dissociates into monomers. At high concentrations ($\geq$100 μM), reduction of $\pi-\{\mathbf{1}\}_2^{2+}$ or $\pi-\{\mathbf{2}\}_2^{2+}$ induces another dimerization reaction, which we attribute to the formation of a σ-bond between the radical tatpp ligands and is accompanied by the appearance of a new peak in the absorption spectrum at 535 nm. This new σ-dimer can undergo one additional tatpp based reduction to form σ-$\{\mathbf{1}\}_2^0$ or σ-$\{\mathbf{2}\}_2^0$, in which the tatpp-bridged assembly is the site of all four reductions. Finally, potentials negative of −1.2 V result in the electroreduction of the bpy or phen ligands for complexes $\mathbf{1}^{2+}$ or $\mathbf{2}^{2+}$, respectively. For the latter complex $\mathbf{2}^{2+}$, this process is accompanied by the formation of an electrode adsorbed species.

Introduction

Ruthenium complexes of pyridyl polyazine ligands such as dppz, tpphz, and tatpp (see Figure 1) have garnered considerable attention due to the unusual acceptor properties of these ligands. Dppz complexes are know to act as molecular light switches which luminesce upon intercalation into DNA or in nonprotic solvents,[1−6] and a number of studies have examined the mechanism by which the luminescent is turned on and off.[7−16] Tpphz complexes behave in a similar manner with DNA and for both dppz and tpphz, the interplay of two energetically similar acceptor orbitals (one centered on the bipyridine-like portion(s) of the ligands and one centered on the phenazine-like portion of the ligands) are responsible for their unusual luminescent behavior.[17−22]

Ruthenium complexes of the tetraazatetrapyridopentacene (tatpp) ligand also exhibit some remarkable properties both in their photochemistry and in their interactions with DNA. Although these complexes are nonluminescent,[23] the dinuclear ruthenium(II) complexes, $[(bpy)_2Ru(tatpp)Ru(bpy)_2]^{4+}$ ($\mathbf{3}^{4+}$) and $[(phen)_2Ru(tatpp)Ru(phen)_2]^{4+}$ ($\mathbf{4}^{4+}$), are photochemically reactive and both undergo multiple tatpp ligand-based reductions upon visible light irradiation in the presence of sacrificial donors.[24−26] The phenanthroline complex $\mathbf{4}^{4+}$ has also shown intriguing biological activity in that its doubly reduced form ($\mathbf{4}^{2+}$) cleaves DNA by a mechanism that appears to involve a carbon-centered radical intermediate.[27] The ability of $\mathbf{4}^{4+}$ to photochemically generate and store up to two reducing equivalents on the tatpp ligand opens a possible pathway by which important multi-electron reactions, such as proton reduction to H_2, may be driven more efficiently using light as the energy

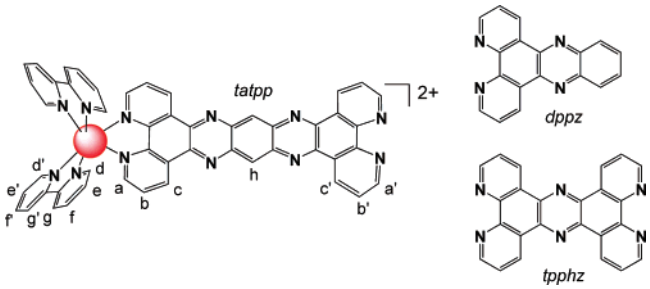

Figure 1. Drawing of $[(bpy)_2Ru(tatpp)]^{2+}$ ($\mathbf{1}^{2+}$) with hydrogens labeled for NMR analysis and the related dppz and tpphz ligands.

[†] The University of Texas at Arlington.
[‡] INIFTA-CONICET.

10.1021/jp0770099 CCC: $40.75
Published on Web 01/03/2008

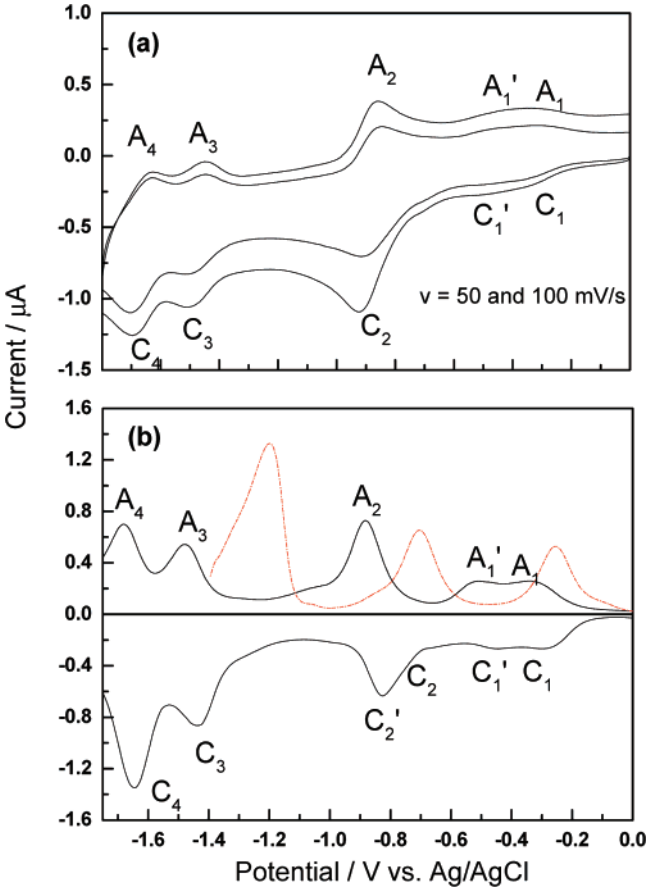

Figure 2. (a) CV of 20 μM complex $\mathbf{1}^{2+}$ in acetonitrile obtained at 50 and 100 mV/s and (b) DPV of 20 μM $\mathbf{1}^{2+}$ recorded at a glassy carbon disk electrode (0.018 cm^2) in acetonitrile/0.1 M $NBu_4{}^nPF_6$ at 293 K. For comparison, a DPV anodic profile of complex $\mathbf{3}^{4+}$ is overlaid (dash line). DPV profiles were obtained with pulse amplitude = 0.01 V, step size = 0.001 V, pulse duration = 0.05 s, and pulse period = 0.2 s.

source. Interest in chemical systems for harvesting solar energy has increased considerably in the past few years[28−33] and only a few molecular systems have shown the ability to generate multiple reducing or oxidizing equivalents via a photochemical process.[25,34−41]

Although we have extensively examined the redox chemistry of $\mathbf{4}^{4+}$ and the associated spectral changes accompanying reduction and protonation in both aqueous and acetonitrile solutions, we have only recently examined mononuclear Ru(II)-tatpp complexes, $[(bpy)Ru(tatpp)]^{2+}$ ($\mathbf{1}^{2+}$) and $[(phen)Ru(tatpp)]^{2+}$ ($\mathbf{2}^{2+}$). A structural drawing of complex $\mathbf{1}^{2+}$ is shown in Figure 1. The preparation of phenanthroline complex$^2[PF_6]_2$ was first reported in 1996 by Lehn and co-workers;[42] however, no absorption or electrochemical data were given. In this report, we describe the redox properties and associated spectral changes seen during the chemical and electrochemical reduction of $\mathbf{1}^{2+}$ and $\mathbf{2}^{2+}$ focusing specifically on the processes associated with tatpp-centered reductions. The large, planar aromatic structure of the tatpp ligand leads to concentration dependent aggregation in solution that not only affects the redox chemistry but also can lead to the formation of new covalent bonds between complexes during the reduction of more concentrated solutions. Reduction of the coordinated tatpp ligand in these aggregates leads to formation of localized "radical anions", which can be reactive toward dimerization.[43−48] The speciation and mechanistic pathways of the electroreduction process were corroborated via digital simulation of the voltammetric results and are presented herein.

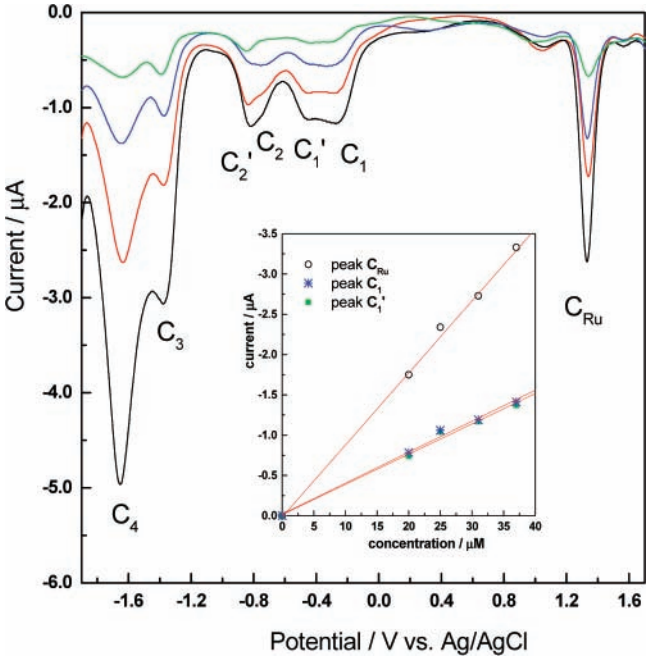

Figure 3. Effect of concentration on the negative-going DPV of $\mathbf{2}^{2+}$ (0.0 to −1.7 V) recorded at a glassy carbon disc electrode (0.018 cm^2) in acetonitrile/0.1 M $NBu_4{}^nPF_6$ at 293 K. Other conditions as in Figure 2. Inset: a linear correlation between peak heights and concentration for complex $\mathbf{2}^{2+}$ is shown for peaks C_1, $C_{1'}$, and C_{Ru}.

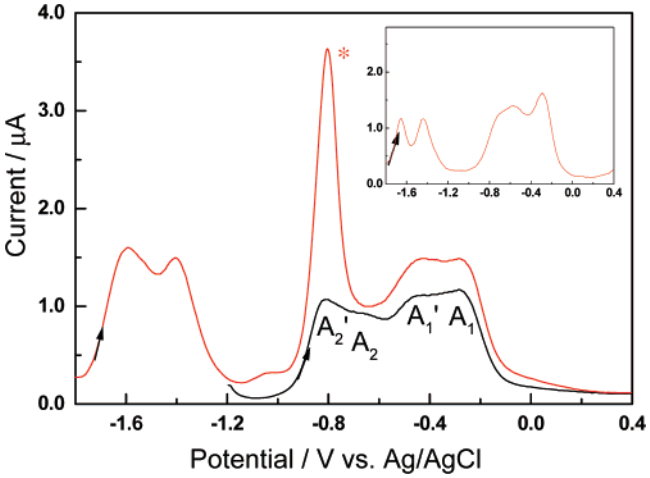

Figure 4. Effect of cathodic limit on the DPV of $\mathbf{2}^{2+}$ (35 μM) recorded at a glassy carbon disk electrode in acetonitrile/0.1 M $NBu_4{}^nPF_6$. The asterisk indicates a stripping peak. Inset: the DPV profile for complex $\mathbf{1}^{2+}$ (120 μM) under the same experimental conditions is included for comparison.

Experimental Section

The mononuclear ruthenium complex $\mathbf{2}[PF_6]_2$ was prepared as described in the literature.[42] The relate bpy analogue, $\mathbf{1}[PF_6]_2$, could be prepared in an identical manner using $[(bpy)_2Ru(1,10\text{-phenanthroline-5,6-dione}][PF_6]_2$[49] in place of $[(phen)_2Ru(1,10\text{-phenanthroline-5,6-dione}][PF_6]_2$.

Electrochemical data were gathered by using a cyclic (CV) and differential pulse voltammograms (DPV) on a PC-controlled potentiostat (CH Instruments, electrochemical analyzer). A single-compartment, three-electrode electrochemical cell was used with a glassy carbon disk as a working electrode (d = 1.5 mm, Cypress) polished with a 0.05 μm alumina paste, a Pt wire auxiliary electrode and a nonleak Ag/AgCl, saturated

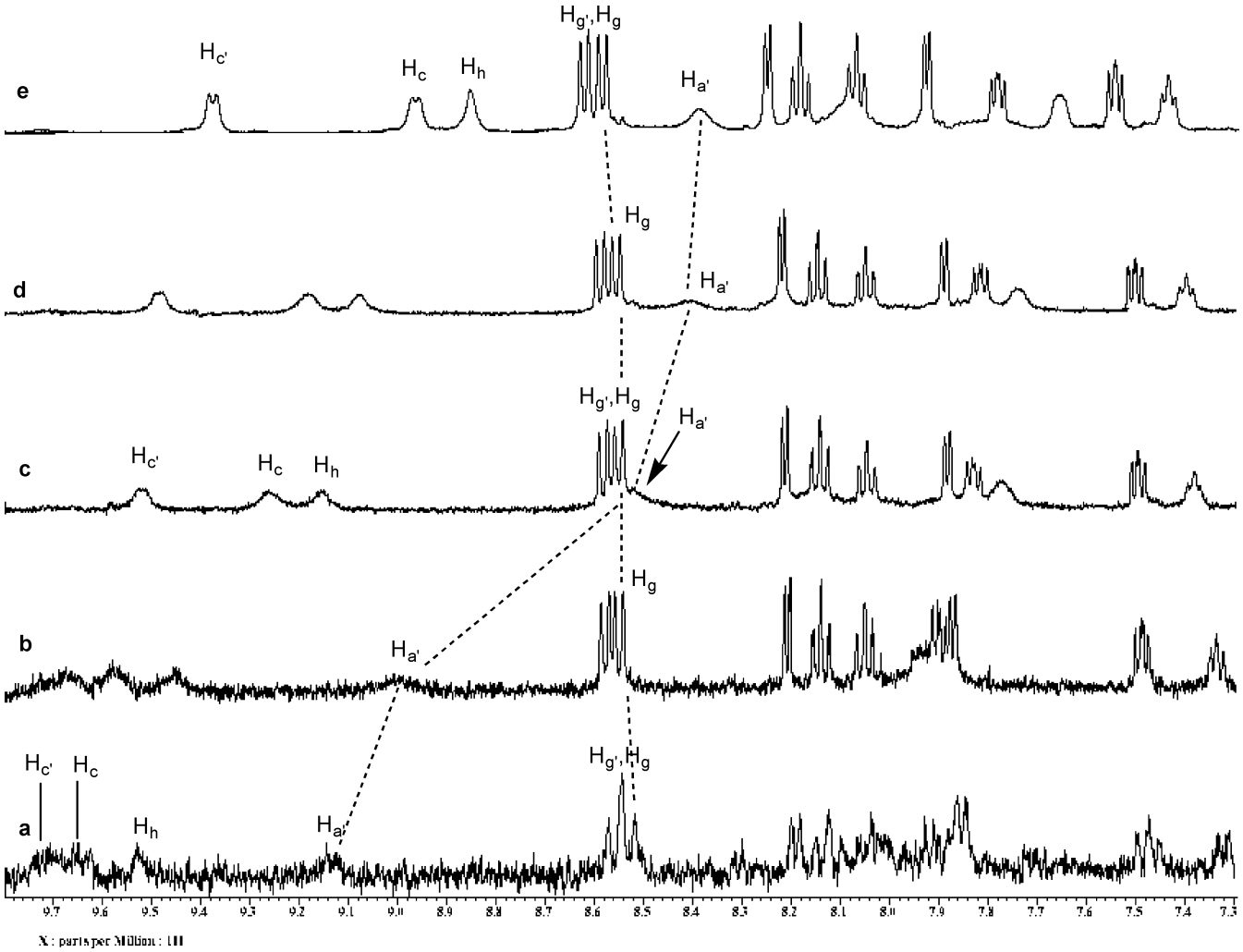

Figure 5. ^{1}H NMR spectra of $\mathbf{1}^{2+}$ in CD_3CN at 90 μM (a), 180 μM (b), 1500 μM (c), 3000 μM (d), and 5000 μM (e), respectively.

KCl (Cypress) reference electrode. All potentials were measured and are quoted vs a Ag|AgCl|saturated KCl reference electrode.

Electronic absorption spectra were measured on a Hewlett-Packard UV−vis spectrophotometer (model 8453) linked to a PC. The spectroelectrochemical (SEC) measurements were carried out with a quartz thin-layer cell containing a gold mesh as working electrode placed inside a 1 cm path quartz cuvette containing ca. 0.5 mL of the mononuclear ruthenium complex solution (20−200 μM). The solution was allowed to fill the thin-layer space, where the gold mesh was located, by capillary action.[24] The counter electrode (platinum wire) and the Ag/Ag^+ quasi-reference electrode were laterally located in the quartz cuvette, close to the capillary slit. The solvent acetonitrile (MeCN, Aldrich) was dried on alumina and distilled under nitrogen *before* use. The supporting electrolyte Bu_4NPF_6 (Aldrich) was dried overnight under vacuum at 60 °C and stored under nitrogen. Other details of the instrumentation for the UV−vis spectroelectrochemistry are given elsewhere.[24]

Simulations of electrochemical data were carried out using the DigiSim software (Bioanalytical Systems).

Results

A. Cyclic Voltammetry and Differential Pulse Voltammetry in Acetonitrile. Cyclic (CV) and differential pulse voltammograms (DPV) of complexes $\mathbf{1}^{2+}$ and $\mathbf{2}^{2+}$ were recorded in acetonitrile with 0.1 M $NBu^n_4PF_6$ as supporting electrolyte (Figures 2−4). As there are changes observed in the peak shape as a function of concentration due to aggregation, the half-wave potentials and the number of electrons (n) for each couple are reported in Table 1 for relatively low concentrations (20 μM). The values for n were obtained by comparison of peak heights with the $Ru^{2+/3+}$ couple, which served as an internal control. As the aggregation is postulated to give rise to $\pi-\pi$ stacked assemblies, Table 1 includes entries for these dimers, π-$\{\mathbf{1}\}_2^{4+}$ and π-$\{\mathbf{2}\}_2^{4+}$, as well as our assignment of the localized site of the reduction. For comparison the data for the related ruthenium complexes, $\mathbf{3}^{4+}$ and $\mathbf{4}^{4+}$, are also included in Table 1.

Figure 2 contains a representative CV (Figure 2a) and DPV (Figure 2b) data for complex $\mathbf{1}^{2+}$ in the 0.0 to −1.8 V potential window. As seen in both the CV and DPV, we observe two small, partially overlapped, waves (C_1 and C_1') in the cathodic scan at −0.31 and −0.45 V, respectively. This is followed by a larger peak (C_2) at −0.82 V; the latter is in fact made of two components (C_2 and C_2'). At more negative potentials, two other peaks (C_3 and C_4) are neatly displayed in both CV and DPV data, although better resolution is achieved with the DPV technique. The anodic scan shows the corresponding oxidation peaks (now labeled A_4 thought A_1) showing all the processes are reversible. For comparison, the DPV data for an anodic scan of the dimer $\mathbf{3}^{4+}$ is overlaid (dashed line) with that of the monoruthenium complex $\mathbf{1}^{2+}$ in Figure 2a. Complex $\mathbf{3}^{4+}$ shows three well-separated electrode processes present in a 1:1:2 ratio of peak heights. All of these redox processes have been assigned

TABLE 1: Electrochemical Data for Complexes $\mathbf{1}^{2+}$ and $\mathbf{2}^{2+}$ (as the Pf_6^- Salts) in Acetonitrile at Complex Concentration of 20 μM

compound	E_f (n)	couple
$\mathbf{1}^{2+}$/p-$\{\mathbf{1}\}_2^{4+}$	+1.35 (**1**)	$[(bpy)_2Ru^{3+/2+}(tatpp)]^{3+/2+}$
π-$\{\mathbf{1}\}_2^{4+}$	−0.31 (0.5)	$[(bpy)_2Ru^{2+}(tatpp^{0/-1})\cdots(tatpp)Ru^{2+}(bpy)_2]^{4+/3+}$
π-$\{\mathbf{1}\}_2^{4+}$	−0.47 (0.5)	$[(bpy)_2Ru^{2+}(tatpp^{-1})\cdots(tatpp^{0/-1})Ru^{2+}(bpy)_2]^{3+/2+}$
	−0.85 (1)	$[(bpy)_2Ru^{2+}(tatpp^{-1/-2})]^{1+/0}$
	−1.46 (1)	$[(bpy^{0/-1})(bpy)Ru^{2+}(tatpp^{-2})]^{0/-1}$
	−1.66 (1)	$[(bpy^{-1})(bpy^{0/-1})Ru^{2+}(tatpp^{-2})]^{-1/-2}$
$\mathbf{2}^{2+}$/p-$\{\mathbf{2}\}_2^{4+}$	+1.33 (1)	$[(phen)_2Ru^{3+/2+}(tatpp)]^{3+/2+}$
π-$\{\mathbf{2}\}_2^{4+}$	−0.30 (0.5)	$[(phen)_2Ru^{2+}(tatpp^{0/-1})\cdots(tatpp)Ru^{2+}(phen)_2]^{4+/3+}$
π-$\{\mathbf{2}\}_2^{4+}$	−0.45 (0.5)	$[(phen)_2Ru^{2+}(tatpp^{-1})\cdots(tatpp^{0/-1})Ru^{2+}(phen)_2]^{3+/2+}$
	−0.83 (1)	$[(phen)_2Ru^{2+}(tatpp^{-1/-2})]^{1+/0}$
	−1.38 (1)	$[(phen^{0/-1})(phen)Ru^{2+}(tatpp^{-2})]^{0/-1}$
	−1.59 (1)	$[(phen^{-1})(phen^{0/-1})Ru^{2+}(tatpp^{-2})]^{-1/-2}$
$\mathbf{3}^{4+}$	+1.39 (2)	$[(bpy)_2Ru^{3+/2+}(tatpp)Ru^{3+/2+}(bpy)_2]^{6+/4+}$
	−0.19 (1)	$[(bpy)_2Ru^{2+}(tatpp^{0/-1})Ru^{2+}(bpy)_2]^{4+/3+}$
	−0.69 (1)	$[(bpy)_2Ru^{2+}(tatpp^{-1/-2})Ru^{2+}(bpy)_2]^{3+/2+}$
	−1.32 (2)	$[(bpy)_2Ru^{2+}(tatpp^{-2/-4})Ru^{2+}(bpy)_2]^{2+/0}$
$\mathbf{4}^{4+}$	+1.41 (2)	$[(phen)_2Ru^{3+/2+}(tatpp)Ru^{3+/2+}(phen)_2]^{6+/4+}$
	−0.22 (1)	$[(phen)_2Ru^{2+}(tatpp^{0/-1})Ru^{2+}(phen)_2]^{4+/3+}$
	−0.71 (1)	$[(phen)_2Ru^{2+}(tatpp^{-1/-2})Ru^{2+}(phen)_2]^{3+/2+}$
	−1.28 (2)	$[(phen)_2Ru^{2+}(tatpp^{-2/-4})Ru^{2+}(phen)_2]^{2+/0}$

as tatpp ligand-based reductions in $\mathbf{3}^{4+}$ corresponding to two one-electron reductions ($tatpp^{0/1-}$, $tatpp^{0/1-}$) and one two-electron reduction ($tatpp^{2-/4-}$).[24] The two one-electron couples in complex $\mathbf{3}^{4+}$ are shifted to more positive potentials[24] compared to the corresponding A_2 and A_1'/A_1 peaks in the DPV for $\mathbf{1}^{2+}$, which is not unusual given the higher overall charge for $\mathbf{3}^{4+}$. Noticably, the two-electron couple seen in complex $\mathbf{3}^{4+}$ at ∼−1.29 V is absent in the mononuclear complex $\mathbf{1}^{2+}$. Presumably, the lower overall charge on $\mathbf{1}^{2+}$ makes the 4-fold reduction of the tatpp ligand inaccessible in this potential window.

Figure 3 shows the DPV profiles for complex $\mathbf{2}^{2+}$ as a function of concentration in the range 20−40 μM. Only the cathodic scans are shown and the potential window is extended to include the $Ru^{2+/3+}$ couple (C_{Ru}) to use it as an internal control to relate the current magnitude with the number of electrons in the couple. At low concentrations, these data mirror those seen for $\mathbf{1}^{2+}$; however, as the concentration is increased, the C_2' peak begins to split (C_2) and the intensity drops to that of the C_1/C_1' peaks. For both mononuclear complexes, $\mathbf{1}^{2+}$ and $\mathbf{2}^{2+}$, the following trends can be observed: (i) Peaks C_1 through C_2' are located at the same potentials supporting our assignment of these as being associated with the common tatpp ligand. (ii) Peaks C_1 and C_1' increase linearly as a function of concentration (Figure 3 inset) with half the slope of the corresponding plot for peak C_{Ru}. (iii) Peak C_2 is hardly discernible at the lowest concentration (20 μM) yet it nearly reaches the height of C_2' at 40 μM (Figure 3). (iv) Peak C_2' is no longer observed at concentrations higher than 200 μM (data not shown). (v) Peaks C_3 and C_4 have a different intensity ratio and are located at different potentials for each complex thus signaling the electroreduction of the bipyridine and phenanthroline respectively.

The complexes $\mathbf{1}^{2+}$ and $\mathbf{2}^{2+}$ do show some important differences, as demonstrated in Figure 4, which illustrates the effect of the negative potential limit on the anodic DPV response of complex $\mathbf{2}^{2+}$. When the anodic DPV scan starts at −1.8 V for $\mathbf{2}^{2+}$, a potential limit that includes the phenanthroline electroreduction, a sharp oxidation peak at −0.8 V (indicated with *) is observed. Under identical conditions with $\mathbf{1}^{2+}$, no such sharp peak is seen (see Figure 4 inset). If the anodic DPV scan for $\mathbf{2}^{2+}$ is started at −1.2 V, which is before the phenanthroline electroreduction region, the sharp intense peak is absent and instead four oxidation processes (A_1, A_1', A_2, and $A_{2'}$) complementary to the cathodic peaks (C_1, C_1', C_2, and $C_{2'}$) are observed. A similar phenomenon is observed in $[Ru(phen)_3]^{2+}$ in which a sharp anodic peak is observed after electroreduction of phenanthroline ligand. Here, the new peak was explained as being related to desorption of the adsorbed reduced species on the working electrode.[50] Similar adsorption features have also been reported in others complexes, especially when phenanthroline-based ligands were used.[51−53]

B. Concentration-Dependence of ^{1}H NMR Spectra of Complex $\mathbf{1}^{2+}$. Figure 5 contains representative ^{1}H NMR spectra of complex $\mathbf{1}^{2+}$ as a function of concentration in CD_3CN. The resonant absorption peaks of the various hydrogens in the complex are labeled as in Figure 1. Upon closer inspection of the data, it is clear that the peaks associated with the tatpp ligand are by far the most perturbed upon changing concentration. For example, $H_{a'}$ is located at the open end of the tatpp ligand away from the sterically crowded Ru center and H_g is located at the 4 position of the bpy ligands. As seen in Figure 5 and highlighted by the dashed lines, $H_{a'}$ shifts by ∼0.8 ppm upfield whereas H_g only shifts by less than 0.1 ppm and shifts upfield. The magnitude and upfield shift of the tatpp protons are characteristic of the formation of $\pi-\pi$ stacked aggregates.[22,49,53−56] Due to the large, planar surface area and the magnitude to the change in chemical shift, it seems logical that the $\pi-\pi$ aggregates are formed by stacking of the tatpp ligands. Although we do not know the size of the aggregate with certainty, $\pi-\pi$ dimers, such as π-$\{\mathbf{1}\}_2^{4+}$, can easily form without the additional steric or electrostatic crowding expected for larger assemblies containing the $\{Ru(bpy)_2\}^{2+}$ or $\{Ru(phen)_2\}^{2+}$ moieties. Contrasting with the $\pi-\pi$ stacking behavior of $\mathbf{1}^{2+}$, the ^{1}H NMR spectra of the related dinuclear complex ($\mathbf{3}^{4+}$) in CD_3CN do not show any concentration dependence.

C. UV−Vis Absorption Spectra of Chemically Reduced Species. The electronic spectra of the dinuclear complexes $\mathbf{3}^{4+}$ and $\mathbf{4}^{4+}$ are known to undergo significant and characteristic changes in the visible and near IR region upon one and two-electron reduction of the central tatpp ligand.[24] The electronic spectra of $\mathbf{1}^{2+}$ and $\mathbf{2}^{2+}$ were found to behave similarly as shown in Figure 6 for complex $\mathbf{1}^{2+}$. In this experiment, cobaltocene was used as a strong one-electron reducing agent (−1.0 V vs Ag|AgCl|saturated KCl in acetonitrile) and thus thermodynamically capable of generating reduced species associated with the C_1 through C_2' electrochemical processes but not the C_3 and

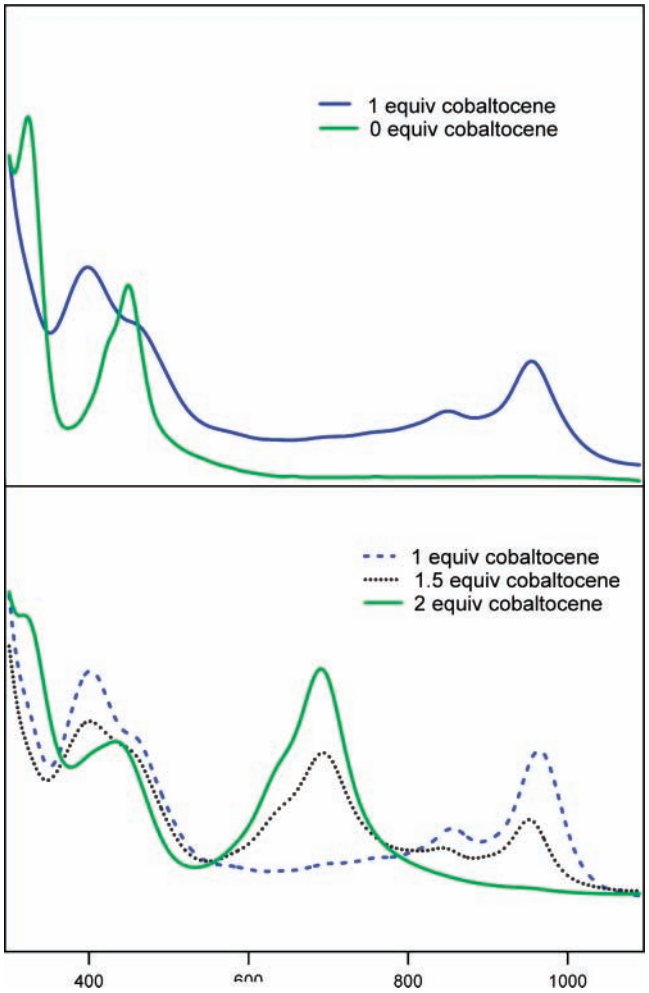

Figure 6. UV−visible electronic spectra of $\mathbf{1}^{2+}$ (18 μM) in acetonitrile obtained before and after the addition of 1.0, 1.5, and 2.0 equiv of cobaltocene. Top panel: absorbance changes observed after addition of 1.0 equiv of cobaltocene. Bottom panel: subsequent absorbance changes seen upon adding an additional 0.5 equiv (1.5 equiv total) and 1.0 (2.0 equiv total) of cobaltocene.

C_4 reductions (see Figures 2 and 3). As seen in Figure 6, complex $\mathbf{1}^{2+}$ shows two strong absorptions in the 300−1100 nm region at 320 nm and at 453 nm. The Zn(II) adduct of tatpp was previously shown to have two tatpp LC transitions at 330 and a structured band at 444 nm and thus we can assign the 330 nm band of complex $\mathbf{1}^{2+}$ as a tatpp LC band.[26] The 453 nm peak is composed of two overlapping peaks as evidenced by the shoulder on the high-energy side; one associated to a tatpp LC transition (at 444 nm) and the other being the Ru dπ-tatpp pπ MLCT transition, which has a maximum (ca. 450 nm) close to that observed for $[Ru(bpy)_3]^{2+}$.

As seen in Figure 6 (top panel), addition of one equivalent of cobaltocene to $\mathbf{1}^{2+}$ shifts the 320 nm peak to 403 nm and gives rise to a strong new structured peak in the near-IR at 855 and 955 nm. The structured band in the near IR of monoreduced species $\mathbf{1}^{\bullet+}$ is very similar to that observed for the monoreduced version of complexes $\mathbf{3}^{4+}$ and $\mathbf{4}^{4+}$, which supports our assignment of this as being a tatpp-centered reduction. Upon addition of 1.5 and then a total of 2 equiv of cobaltocene to $\mathbf{1}^{2+}$ the spectra change as shown in Figure 6 (bottom panel). Addition of 1.5 equiv of cobaltocene is shown to decrease the bands at 855 and 955 nm and to lead to a new band at 685 nm with a shoulder at 630 nm, indicating the progressive electron uptake by the complex. These changes continue and reach their limit with addition of 2 equiv of cobaltocene, giving finally the absorption spectrum of the double reduced species, $\mathbf{1}^{0}$. The spectral changes here also are congruent with those observed for double-reduction of $\mathbf{3}^{4+}$ and $\mathbf{4}^{4+}$ and are again assigned to reduction of the tatpp ligand, in this case by 2 electrons.

D. Spectroelectrochemistry. A spectroelectrochemical cell was used to observe the electronic absorption changes of complex $\mathbf{2}^{2+}$ upon electrochemical reduction. The spectroelectrochemical data were obtained by collecting transmittance spectra in a capillary slit cell containing the working electrode (gold mesh). The spectra were collected during a linear scan at 5 mV/s in the potential window from 0.0 to −1.2 V using a 120 μM complex $\mathbf{2}^{2+}$ in acetonitrile. The negative potential limit was purposely kept at −1.2 V to avoid complications due to adsorption processes occurring in the potential range of phenanthroline reduction (vide supra, Figure 4).

The spectral evolution is shown in Figure 7 and is separated into three frames: frame a corresponds to potentials encompassing voltammetric peaks C_1 and C_1', frame b is related to peak C_2, and frame c to peak C_2', respectively. The first spectrum in frame a corresponds to the initial complex $\mathbf{2}^{2+}$, which is recognized by two main bands at 453 and 320 nm. During the C_1 and C_1' electroreduction processes, the bands at 453 and 320 nm are seen to decrease attended by the emerging of three new bands, one at 403 and a pair of very broad bands in the 800−950 nm range. These spectral changes mirror those seen in the cobaltocene reduction of $\mathbf{1}^{2+}$ to $\mathbf{1}^{\bullet+}$ and indicate monoreduction of the tatpp portion of the complex.

The spectral evolution accompanying voltammetric peak C_2 (frame b in Figure 7) is characterized by a partial bleaching and red-shifting of the near-IR peaks and the appearance of a new broad band peaking at 535 nm. This new band was not found in the chemical reduction with cobaltocene (Figure 6). Finally, in the potential region of voltammetric peak C_2' (frame c in Figure 7), the band at 535 nm remains unchanged and a new pair of bands at 630 and 685 nm progressively grows in while the near-IR band pair bleaches. The bands at 630 and 685 nm, are characteristic of double-reduction of the tatpp ligand in the dinuclear complexes (e.g., $\mathbf{3}^{4+}$ and $\mathbf{4}^{4+}$)[24] and is in good agreement with the changes observed for $\mathbf{1}^{0}$ obtained by cobaltocene reduction (Figure 6b). The spectroelectrochemical behavior of complex $\mathbf{1}^{2+}$ is identical to that for $\mathbf{2}^{2+}$ and therefore also shows the appearance of a new band at 535 nm. Again, this new peak was not observed in any of the cobaltocene reductions nor in any of the data (chemical reduction or SEC) for $\mathbf{3}^{4+}$ and $\mathbf{4}^{4+}$. Our assignment of this peak is deferred to the discussion.

Discussion

By most measures, the properties of the bpy and phen complexes, $\mathbf{1}^{2+}$ and $\mathbf{2}^{2+}$, are nearly identical. Both complexes show aggregation behavior in solution and both exhibit spectral changes upon reduction that correspond with the initial site of reduction by 1 or 2 electrons being on the tatpp ligand. The biggest difference between the two being the tendency of the phen analogue $\mathbf{2}^{2+}$ to be electroadsorbed onto the electrode surface when the phenanthroline ligands are reduced.

In comparison with the dinuclear complexes, $\mathbf{3}^{4+}$ and $\mathbf{4}^{4+}$, these mononuclear Ru(II) complexes show one unique property, which is the tendency to form $\pi-\pi$ stacked dimers in acetonitrile as indicated by the NMR data.[57] Such stacking behavior can be induced in the dinuclear complexes in water but any such association in acetonitrile is not detected. Presumably this

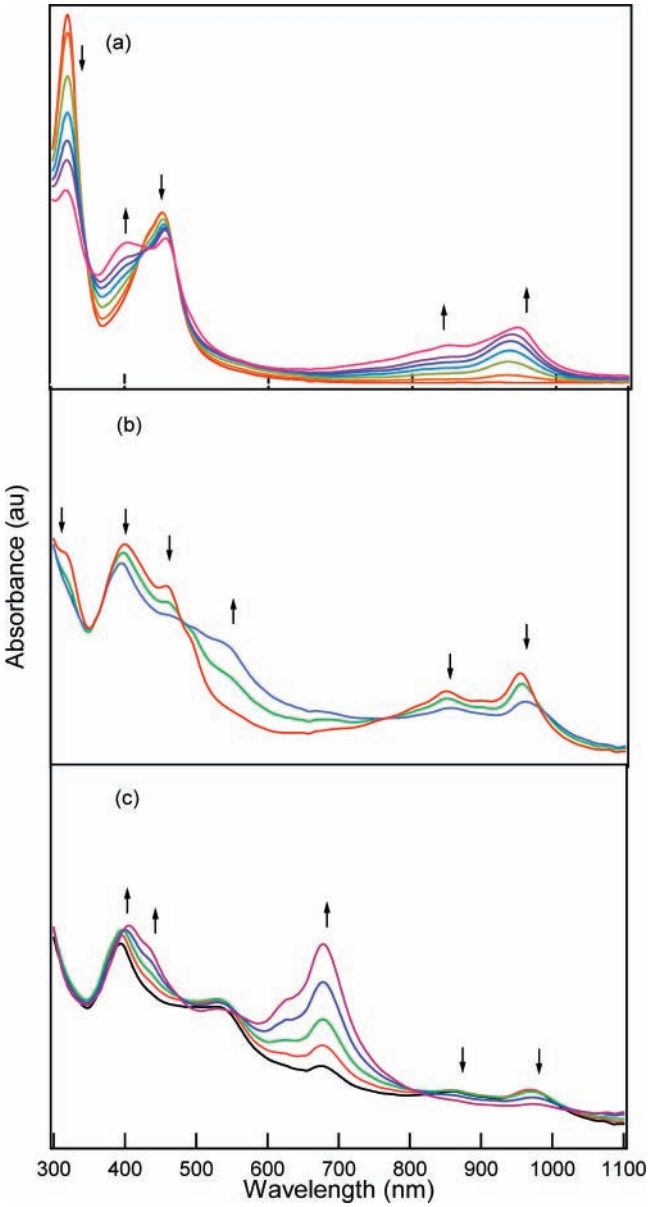

Figure 7. Spectroelectrochemistry of $\mathbf{2}^{2+}$ (120 μM) in acetonitrile containing 0.1 M $NBu_4^nPF_6$ using a capillary slit cell. Spectra were collected during a negative-going potential scan at 5 mV/s in the +0.2 to −1.2 V potential range. For the sake of clarity, only a selected subset of spectra is shown in the potential region of peaks C_1 and $C_{1'}$ (frame a), C_2 (frame b), and $C_{2'}$ (frame c) respectively.

is because the electrostatic repulsion is greater in these +4 complexes and the steric congestion about the tatpp ligands is greater thus limiting the aromatic surface area available for stacking.

The $\pi-\pi$ dimerization constant ($K_{\pi-\text{dim}}$) for $\mathbf{1}^{2+}$ can be extracted from the NMR data plotted in Figure 8a for the $H_{a'}$ NMR peak. The fitting of the NMR data uses the expressions given in eqs 1−4, where M is the monomer $\mathbf{1}^{2+}$, D is the dimer $\{\mathbf{1}\}_2^{4+}$, and $K_{\pi-\text{dim}}$ is the dimerization constant given in eq 2.[58]

$$\mathbf{M} + \mathbf{M} \longleftrightarrow \mathbf{D} \tag{1}$$

$$K_{\pi-\text{dim}} = [\text{D}]/[\text{M}]^2 = f_\text{D}/2f_\text{M}^2[\text{M}]_i \tag{2}$$

The mole fraction of monomer (f_M) and dimer (f_D) were calculated using eqs 3 and 4, where δ_0 is the chemical shift of

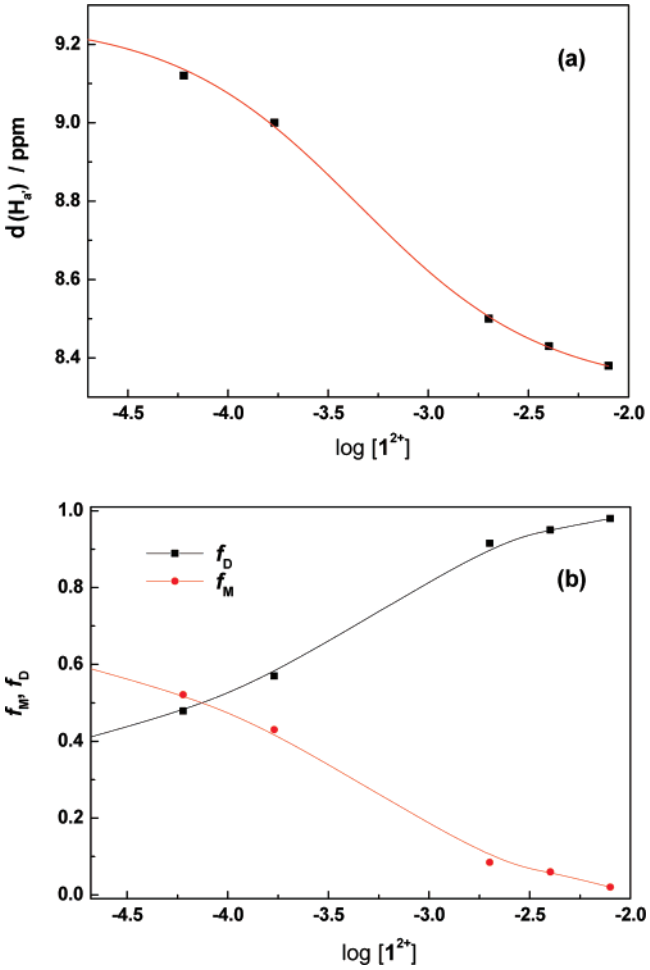

Figure 8. Analysis of the ^{1}H NMR data in Figure 5 for $\mathbf{1}^{2+}$ for the determination of the $K_{\pi-\text{dim}}$: (a) change in chemical shift for the $H_{a'}$ peak as a function of $\mathbf{1}^{2+}$ concentration in acetonitrile at 25 °C; (b) calculated mole fraction of monomer and π-dimer.

free monomers, δ_S is the chemical shift of the fully stacked species, and δ is the shift at each experimental concentration.

$$f_\text{M} = (\delta - \delta_s)/(\delta_0 - \delta_s) \tag{3}$$

$$f_\text{D} = (\delta_0 - \delta)/(\delta_0 - \delta_s) \tag{4}$$

A plot of f_M and f_D is shown in Figure 8b and the $K_{\pi-\text{dim}}$ was calculated to be 2×10^4 M^{-1} using the values for δ_0 and δ_s of 9.45 and 8.38 ppm, respectively. The value of the dimerization constant is similar to that for $\pi-\pi$ stacks of neutral compounds and much larger than that observed in another ruthenium complex, $[(bpy)_2Ru(bqpy)Ru(bpy)_2]^{4+}$ (where bqpy is bis-{dipyrido[3,2-*f*:2′,3′-*h*]quinoxalo][2,3-*e*:2′,3′-l]pyrene) at 830 M^{-1} in MeCN. The larger value for $\mathbf{1}^{2+}$ is to be expected as this complex has lower overall charge.

The presence of the $\pi-\pi$ dimers is also evident in the electrochemical and SEC data. Scheme 1 shows the speciation and reduction pathways observed during the formal reduction of complex $\mathbf{1}^{2+}$ to $\mathbf{1}^0$ as determined by a combination of all the data collected in this work. In this scheme, the $\pi-\pi$ dimer $\{\mathbf{1}\}_2^{4+}$ is the central species, which exhibits unique redox and reactivity properties. Identical dimerization and redox processes are seen to occur in $\mathbf{2}^{2+}$; however, only $\mathbf{1}^{2+}$ will be discussed initially for the sake of simplicity.

As was seen in Figure 2, the first reduction process in complex $\mathbf{1}^{2+}$ is split into two redox process C_1 and C_1', which

SCHEME 1

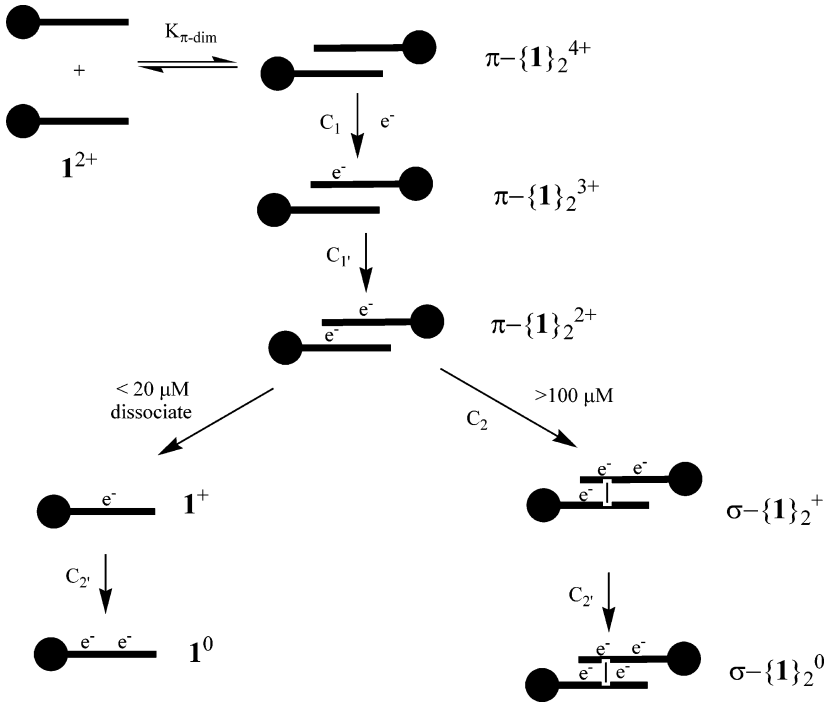

SCHEME 2

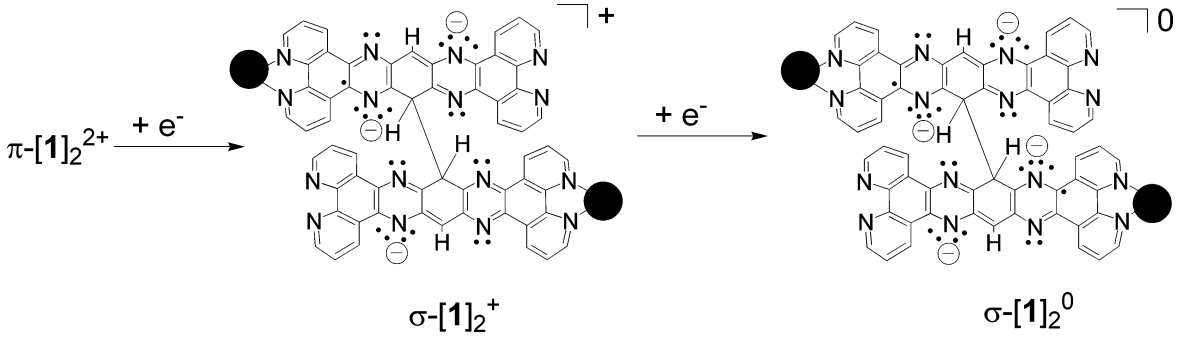

exhibit half the current intensity of a one-electron process. This splitting can be attributed to the dimeric structure, π-$\{\mathbf{1}\}_2^{4+}$, which undergoes two consecutive reductions (C_1 and C_1'), as shown in eqs 5 and 6, and corresponds to sequential reduction

$$\pi\text{-}\{\mathbf{1}\}_2^{4+} + \text{e-} \longleftrightarrow \pi\text{-}\{\mathbf{1}\}_2^{3+} \quad (5)$$

$$\pi\text{-}\{\mathbf{1}\}_2^{3+} + \text{e-} \longleftrightarrow \pi\text{-}\{\mathbf{1}\}_2^{2+} \quad (6)$$

of the two tatpp ligands in the dimer$\{\mathbf{1}\}_2^{4+}$. Similar electrochemical behavior was reported in the voltammetric profiles for other Ru(II) polypyridyl complexes,[59,60] phthalocyanine,[61] and porphyrin complexes,[62] all containing flat aromatic ligands capable of forming dimers and /or aggregates.

Using the $K_{\pi-\text{dim}}$ from the NMR data, the apparent mole fraction of dimer in the electrochemistry experiments is only expected to be between 0.40 and 0.52. However, the CV and DPV data clearly show the π-dimer as the majority species, which we speculate is due to the high ionic strength of the electrochemical solution (0.1 M $Bu_4N{\cdot}PF_6$ supporting electrolyte) compared to the NMR solutions (no added electrolyte). The presence of electrolyte favors $\pi-\pi$ stacking by both masking the cationic charge of $\mathbf{1}^{2+}$ and increasing the ionic strength of the solution.

Another possibility is indicated in reactions 7 and 8 in which the initial one-electron reduction of $\mathbf{1}^{2+}$ (reaction 7) gives rise to a radical species $\mathbf{1}^{\bullet+}$. This radical species (formally a tatpp

$$\mathbf{1}^{2+} + \text{e}^- \longleftrightarrow \mathbf{1}^{\bullet+} \quad (7)$$

$$\mathbf{1}^{\bullet+} + \mathbf{1}^{2+} \longleftrightarrow \pi\text{-}\{\mathbf{1}\}_2^{3+} \quad (8)$$

radical anion) rapidly associates with another $\mathbf{1}^{2+}$ to give the dimer $\{\mathbf{1}\}_2^{3+}$ (reaction 8). This type of dimerization scheme has been reported for dppz radical anions to give $\{\text{dppz}\}_2^{\bullet-}$ dimers[63,64] and for some metalloporphyrins.[65] In the dppz study, the structure of the $\{\text{dppz}\}_2^{\bullet-}$ dimers was not defined so either a $\pi-\pi$ stacked dimer or σ-bond between dppz units is possible. The formation of dimers by reaction 8 has to be fast enough on the electrochemical time scale so that the next electron transfer (at peak $C_{1'}$) would find all of the $\mathbf{1}^{+\bullet}$ already converted to $\{\mathbf{1}\}_2^{3+}$ and ready to receive a second electron to form $\{\mathbf{1}\}_2^{2+}$. If this were the case, the heights of peak C_1 and $C_{1'}$ would behave similarly on DPV profiles. This latter mechanism (reactions 7 and 8) can explain the observed splitting of the initial reduction peak in the CV and DPV data; however, we favor the mechanism indicated in reactions 5 and 6 as the NMR data clearly indicate an appreciable amount of $\pi-\pi$ stacking in the initial solution.

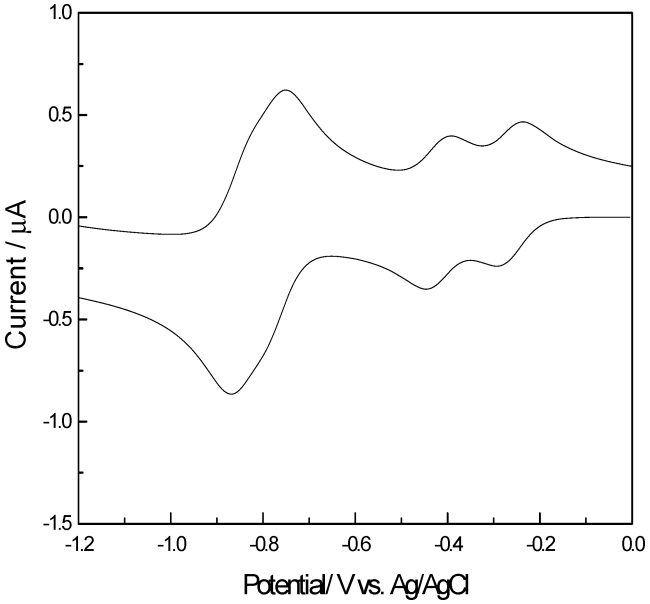

Figure 9. Simulation of a voltammetric profile at 50 mV/s for complex $\mathbf{1}^{2+}$ in the 0.0 to −1.2 V range covering the electroreduction of the tatpp ligand. Simulation parameters are provided in Table 2 and correspond to the experimental data in Figure 2a excluding the electrode processes associated with the bipyridine ligands.

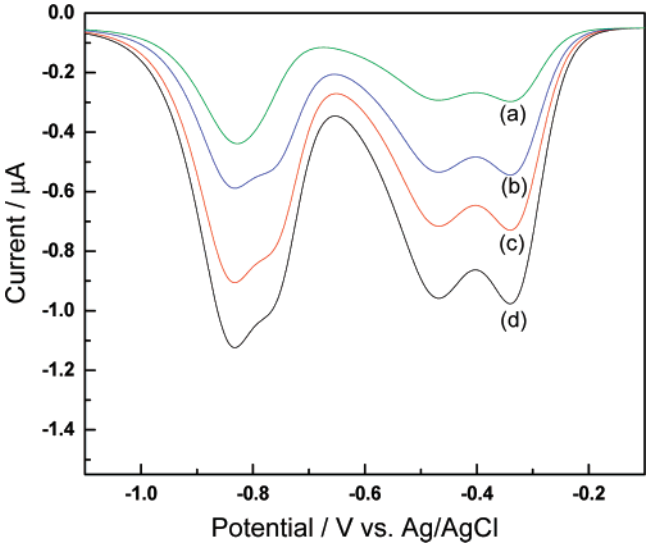

Figure 10. Simulation of current−potential profiles for complex $\mathbf{2}^{2+}$ in the 0.0 V/−1.2 V window for the electroreduction of the tatpp ligand. The four profiles are simulated curves of the experimental data in Figure 3 in the same specified potential window. This simulation was obtained using the proposed mechanism described in Scheme 1. Nominal values of the various simulation parameters are presented in Table 2.

Further support for role of π-$\{\mathbf{1}\}_2^{4+}$ in the speciation of $\mathbf{1}^{2+}$ is seen in the absorbance data obtained in the SEC experiments. The near-IR bands in the SEC (Figure 8 frame a) are seen to red shift during the formation of π-$\{\mathbf{1}\}_2^{3+}$ as could be expected for the larger dimeric structure.[66] Importantly, this red shift is not seen during the first reduction of the dinuclear analogs $\mathbf{3}^{4+}$ and $\mathbf{4}^{4+}$.[24]

Referring back to Scheme 1, once the first two redox processes (C_1 and $C_{1'}$) have occurred the resulting dimer π-$\{\mathbf{1}\}_2^{2+}$ can either dissociate (at low concentrations (<40 μM)) or undergo further redox processes (at higher concentrations (>120 μM)) including, we speculate, formations of a σ-bonded dimer.

First at low concentrations, the next redox process $C_{2'}$ largely appears as a single one-electron reduction of the monomer $\mathbf{1}^{\bullet+}$, as the $C_{2'}$ peak intensity is approximately twice as high as either the C_1 or $C_{1'}$ process (see Figure 2). This redox process is always associated with the appearance of a peak at 685 nm in the absorption spectrum and is characteristic of a doubly reduced tatpp ligand.[24,26] Therefore, we speculate dissociation of the $\pi-\pi$ dimer π-$\{\mathbf{1}\}_2^{2+}$ into monomers (reaction 9), which are then reduced by one electron to form the neutral complex $\mathbf{1}^0$ (reaction 10). Kol and co-workers[59,60] observed a similar dissociation of a $\pi-\pi$ stacked dimer of $[(phen)_2Ru(dibenzoelatin)]^{2+}$ after each dibenzoelatin ligand picked up a single electron.

$$\pi\text{-}\{\mathbf{1}\}_2^{2+} \longleftrightarrow 2\,\mathbf{1}^{\bullet+} \tag{9}$$

$$\mathbf{1}^{\bullet+} + \mathbf{e}^- \longleftrightarrow \mathbf{1}^0 \tag{10}$$

As the concentration of the complex is increased, the DPV profile in the $C_{2'}$ region changes as the C_2 peak becomes more pronounced and the $C_{2'}$ peak shifts slightly positive and begins to merge with C_2. Spectroelectrochemical data covering C_2 first show the appearance of a new species (characterized by a band at 535 nm), which we believe corresponds to the formation of a σ-bond between tatpp ligands in π-$\{\mathbf{1}\}_2^{2+}$ to form σ-$\{\mathbf{1}\}_2^{+}$ (reaction 11). The resulting σ-dimer is then further reduced to form σ-$\{\mathbf{1}\}_2^{0}$ (reaction 12).

$$\pi\text{-}\{\mathbf{1}\}_2^{2+} + \mathbf{e}^- \longleftrightarrow \sigma\text{-}\{\mathbf{1}\}_2^{+} \tag{11}$$

$$\sigma\text{-}\{\mathbf{1}\}_2^{+} + \mathbf{e}^- \longleftrightarrow \sigma\text{-}\{\mathbf{1}\}_2^{0} \tag{12}$$

Formation of a σ-bond is supported by several pieces of inferential evidence. First, we have never observed this peak at 535 nm in the redox chemistry of $\mathbf{3}^{4+}$ and $\mathbf{4}^{4+}$ at any concentration. This new peak at 535 nm is also seen in the spectroelectrochemistry of $\mathbf{2}^{2+}$ supporting our assignment of this process being based on the tatpp portion of the complex. The related $\{dppz\}_2^{\bullet-}$ dimer generated electrochemically also shows a strong new peak in this vicinity (λ_{max} = 565 nm), which could be the related optical transition for σ-bond formation in this dimer.[63,64] Second, as this new peak at 535 nm is growing in, the near-IR bands further red shift and decrease but do not disappear (see Figure 7). The red shift could be due to the increase in conjugation length as the two aromatic systems are linked and the remaining peak intensity would be supportive of at least one-half of the resulting dimer having a formally "singly reduced" tatpp ligand (albeit it modified by the new σ-bond). Once the peak at 535 nm has stopped increasing, the characteristic peak at 685 nm for doubly reduced tatpp ligands grows in, showing that each of the new modified "tatpp" ligands in σ-$\{\mathbf{1}\}_2^{0}$ or σ-$\{\mathbf{2}\}_2^{0}$ is very similar to a doubly reduced tatpp ligand (such as those seen in $\mathbf{1}^0$, $\mathbf{2}^0$, $\mathbf{3}^{2+}$, and $\mathbf{4}^{2+}$). Furthermore, the near-IR bands are completely bleached during this last reduction.

The absorption changes associated with the chemical reduction of $\mathbf{1}^{2+}$ with cobaltocene, shown in Figure 6, show no sign of the 535 nm peak and are nearly identical to the changes seen in the chemical reduction and electroreduction of $\mathbf{4}^{4+}$ to $\mathbf{4}^{3+}$ and $\mathbf{4}^{2+}$.[23,24] This experiment is conducted at low concentration (~15 μM) and thus is expected to favor monomers. The dinuclear complexes $\mathbf{3}^{4+}$ and $\mathbf{4}^{4+}$ show an additional two-electron redox process that has been assigned as the 4-electron reduction of the central tatpp ligand. No additional tatpp-centered reductions are seen in either the doubly reduced

TABLE 2: Parameters Derived in the Simulation of the CV and DPV of $\mathbf{1}^{2+}$ and $\{\mathbf{1}\}_2^{4+}$ Shown in Figures 9 and 10

				electrochemical reaction			
figure	EC method	concentrations[a] and diffusion coefficients[b]	chemical reactions	C_1	$C_{1'}$	C_2	$C_{2'}$
9	CV	$[c_i] = 20\ \mu M$ $[\{1\}_2^{4+}] = 8\ \mu M$ $D(1^{2+}) = 1 \times 10^{-5}$ $D(\{1\}_2^{4+}) = 3 \times 10^{-6}$	$K_{\pi-dim}$[c] $= 8 \times 10^4$	$E_0[1] = -0.26$ V $\alpha = 0.5$ $k(1)$[f] $= 10^{-2}$	$E_0[1'] = -0.42$ V $\alpha = 0.5$ $k(1')$[f] $= 10^{-3}$	$E_0[2] = -0.77$ V $\alpha = 0.5$ $k(2)$[f] $= 10^{-2}$	$E_0[2'] = -0.85$ V $\alpha = 0.5$ $k(2')$[f] $= 10^{1}$
10a	DPV	$[c_i] = 20\ \mu M$ $[\{\mathbf{1}\}_2^{4+}] = 5\ \mu M$ $D(\mathbf{1}^{2+}) = 1 \times 10^{-5}$ $D(\{\mathbf{1}\}_2^{4+}) = 3 \times 10^{-6}$	$K_{\pi-dim} = 5 \times 10^4$ $K_{\sigma-dim} = 2 \times 10^1$ [d] ($k_{f,dim} = 8 \times 10^4$) $K_{diss} = 1 \times 10^2$ [e] ($k_{f,diss} = 7 \times 10^{-1}$)	$E_0[1] = -0.28$ V $\alpha = 0.5$ $k(1)$[f] $= 10^{-2}$	$E_0[1'] = -0.43$ V $\alpha = 0.5$ $k(1)$[c] $= 10^{-3}$	$E_0[2] = -0.78$ V $\alpha = 0.5$ $k(1)$[c] $= 10^{-2}$	$E_0[2'] = -0.85$ V $\alpha = 0.5$ $k(1)$[c] $= 10^{1}$
10b		$[c_i] = 25\ \mu M$ $[\{\mathbf{1}\}_2^{4+}] = 8.5\ \mu M$	same constants as in Figure 10a	$E_0[1] = -0.28$ V	$E_0[1'] = -0.43$ V	$E_0[2] = -0.78$ V	$E_0[2'] = -0.85$ V
10c		$[c_i] = 30\ \mu M$ $[\{\mathbf{1}\}_2^{4+}] = 11.4\ \mu M$	same constants as in Figure 10a	$E_0[1] = -0.28$ V	$E_0[1'] = -0.44$ V	$E_0[2] = -0.77$ V	$E_0[2'] = -0.85$ V
10d		$[c_i] = 38\ \mu M$ $[\{\mathbf{1}\}_2^{4+}] = 16\ \mu M$	same constants as in Figure 10a	$E_0[1] = -0.28$ V	$E_0[1'] = -0.45$ V	$E_0[2] = -0.77$ V	$E_0[2'] = -0.85$ V

[a] $[c_i]$ and $[\{\mathbf{1}\}_2^{4+}]$ are the initial complex concentration and that of the resulting π-dimer species. [b] Diffusion coefficients used for dimeric and monomeric species; they are given in cm^2/s. [c] $K_{\pi-dim} = [[\{\mathbf{1}\}_2^{4+}]/[\mathbf{1}^{2+}]^2$ is the π dimerization equilibrium contant given in M^{-1}. [d] $K_{\sigma-dim}$ and $k_{f,dim}$ are the σ dimerization equilibrium and forward reaction constants respectively. [e] $K_{Diss} = [\mathbf{1}^{\bullet+}]^2/[\{\mathbf{1}\}_2^{2+}]$ and $k_{f,diss}$ is the π-dimer dissociation equilibrium and forward reaction constants respectively. [f] Heterogeneous rate constants for the electrochemical reactions.

monomers, $\mathbf{1}^0$ and $\mathbf{2}^0$, or the quadruply reduced σ-dimers, σ-$\{\mathbf{1}\}_2^0$ or σ-$\{\mathbf{2}\}_2^0$. Presumably, this last two-electron reduction of the tatpp ligand is only possible when both ends of the tatpp ligand are coordinated by $Ru(bpy)_2^{2+}$ or $Ru(phen)_2^{2+}$ fragments.

Scheme 2 shows postulated structures for the σ-bonded dimer after the C_2 and $C_{2'}$ processes. The $\pi-\pi$ stacked dimer situates the two tatpp ligands such that σ-bond formation should be facile upon a simple shift of the tatpp ligands and a twist between the planes of the two ligands upon σ-bond formation. We have linked the two tatpp ligands at the central carbons as this is known to be the site of maximum electron density upon reduction from theoretical calculations.[20] The formation of a σ-bond between many organic and organometallic free radicals is a distinguishing characteristic of their dynamic behavior, irrespective of whether the singly occupied molecular orbital (SOMO) is centered on carbon or heteroatom.[67−72] It is also possible that the $\pi-\pi$ stacked dimer forms a true π-bond between the tatpp ligands as both π-bonded and σ-bonded dimers of radical species are known, with the primary difference being the intermolecular separation of the two joined fragments, which is substantially longer in the π-bonded case.[73−75] In this work, both such structures are possible and we cannot distinguish between the two without additional structural and spectroscopic data. It is interesting to note that the structure for σ-$\{\mathbf{1}\}_2^0$ in Scheme 2 is a diradical that should be detectable by EPR. The difficulty in distinguishing between the two (σ or π) is reflected in that a number of previous studies of dimerization in solution have left open the critical question of the nature of the dimer.[76−78] We are currently working to obtain both structural and EPR data for this system.

Simulations of voltammetric data corroborate the mechanism described by Scheme 1. Figure 9 shows a simulation that was restrained to the potential window encompassing the C_1, $C_{1'}$, C_2, and $C_{2'}$ processes. The best fit of the similated CV to the data in Figure 2a (100 mV/s scan) was obtained with the parameters compiled in Table 2. This gives an equilibrium constant $K_{\pi-dim} = 8 \times 10^4\ M^{-1}$ (see eq 2) for $\mathbf{1}^{2+}$, which is in decent agreement with that obtained from the NMR data given the expected differences due to the presence of an electrolyte in the electrochemical experiments. Similation of cathodic processes C_1, $C_{1'}$, C_2, and $C_{2'}$ in the DPV data of $\mathbf{2}^{2+}$, shown in Figure 3, was performed with the parameters listed in Table 2. The simulations, shown in Figure 10, match well the observed height, shape and evolution of the experimental voltammetric peaks. From this simulation, we also obtain a dimerization constant ($K_{\pi-dim}$) of $5 \times 10^4\ M^{-1}$ for the $\pi-\pi$ stacking and a second dimerization constant for the proposed σ-bond formation (K_{s-dim}) of $20\ M^{-1}$ for $\mathbf{2}^{2+}$. At low concentrations (<20 μM) the electroreduction of monomer species is favored (analogous to the left branch of Scheme 1) leading to the appearance of species $\mathbf{2}^0$ (peak $C_{2'}$) after dissociation of the $\{\mathbf{2}\}_2^{2+}$ dimer. At higher concentrations the further reduction of dimer $\{\mathbf{2}\}_2^{2+}$ (analogous to the right branch of Scheme 1) becomes predominant. The reversibility of the σ-dimerization process could not be examined by SEC as the product precipitates in the thin layer cell and the reverse scan is not interpretable. However, the anodic scan of the DPV, shown in Figure 4, shows that all cathodic peaks have well-defined anodic counterparts (A_1, $A_{1'}$, A_2, and $A_{2'}$) and thus the process appears reversible electrochemically.

Conclusions

The combination of electrochemical, spectroelectrochemical, ^1H NMR data, and digital simulations provides a detailed view of the speciation and redox species involved in the reduction of the mononuclear tatpp complexes, $\mathbf{1}^{2+}$ and $\mathbf{2}^{2+}$. The two complexes display nearly identical absorption spectra in the visible and near-IR region and in their electrochemical behavior concerning the reduction of the tatpp ligand. This long planar ligand gives rise to the formation of $\pi-\pi$ stacked dimers in solution as a function of concentration. The $\pi-\pi$ stacking alters the redox properties of the resulting dimer, especially with respect to the first two reductions, which are largely localized on the tatpp ligands. An overall two-electron reduction of $\mathbf{1}^{2+}$ or $\mathbf{2}^{2+}$ gives rise to vastly different products at high and low concentration. At the low concentrations typical of most UV-visible experiments (<20 mM) for these complexes, the $\pi-\pi$ dimer dissociates after each tatpp ligand in the dimer has been reduced by one electron and the resulting monomer, $\mathbf{1}^{\bullet+}$ or $\mathbf{2}^{\bullet+}$,

accepts a second electron to form the neutral complexes $\mathbf{1}^0$ or $\mathbf{2}^0$. At the higher concertrations typical of a thin-layer SEC experiment (and in the presence of supporting electrolyte) the $\pi-\pi$ dimers, π-$\{\mathbf{1}\}_2^{4+}$ and π-$\{\mathbf{2}\}_2^{4+}$, do not dissociate after tatpp reduction (π-$\{\mathbf{1}\}_2^{2+}$ and π-$\{\mathbf{2}\}_2^{2+}$) but instead undergo what we believe to be σ-bond formation between tatpp ligands to form σ-dimers upon further reduction. These new σ-dimers, σ-$\{\mathbf{1}\}_2^{+}$ and σ-$\{\mathbf{2}\}_2^{+}$, exhibit a unique spectral feature in the absorption spectrum at 535 nm, which is retained even after further reduction to the neutral species σ-$\{\mathbf{1}\}_2^0$ and σ-$\{\mathbf{2}\}_2^0$. This solution speciation is significantly different from that observed for the related dinuclear $\mathbf{3}^{4+}$ complex, in which no indication of larger aggregates are observed in acetonitrile.

Acknowledgment. We thank the National Science Foundation CHE-0518649 (FMM, NRT), the Robert A. Welch Foundation Y-1301(FMM,) and BID 1728/OC-RA, PICT #26195/04 (ROL) for support of this research.

References and Notes

(1) Chambron, J.-C.; Suavage, J.-P.; Amouyal, E.; Kiffi, P. *Nouv. J. Chim.* **1985**, *9*, 527−529.
(2) Friedman, A. E.; Chambron, J.-C.; Sauvage, J.-P.; Turro, N. J.; Barton, J. K. *J. Am. Chem. Soc.* **1990**, *112*, 4960−4961.
(3) Hartshorn, R. M.; Barton, J. K. *J. Am. Chem. Soc.* **1992**, *114*, 5919−5925.
(4) Hiort, C.; Lincoln, P.; Nordén, B. *J. Am. Chem. Soc.* **1993**, *115*, 3448−3454.
(5) Haq, I.; Lincoln, P.; Suh, D.; Norden, B.; Chowdhry, B. Z.; Chaires, J. B. *J. Am. Chem. Soc.* **1995**, *117*, 4788−4796.
(6) Guo, L.-H.; Wei, M.-Y.; Chen, H. *J. Phys. Chem. B* **2006**, *110*, 20568−20571.
(7) Brennaman, M. K.; Alstrum-Acevedo, J. H.; Fleming, C. N.; Jang, P.; Meyer, T. J.; Papanikolas, J. M. *J. Am. Chem. Soc.* **2002**, *124*, 15094−15098.
(8) Olson, E. J. C.; Hu, D.; Hoermann, A.; Jonkman, A. M.; Arkin, M. R.; Stemp, E. D. A.; Barton, J. K.; Barbara, P. F. *J. Am. Chem. Soc.* **1997**, *119*, 11458−11467.
(9) Coates, C. G.; Callaghan, P.; McGarvey, J. J.; Kelly, J. M.; Jacquet, L.; Kirsch-De Mesmaeker, A. *J. Mol. Struc.* **2001**, *598*, 15−25.
(10) Turro, C.; Bossmann, S. H.; Jenkins, Y.; Barton, J. K.; Turro, N. J. *J. Am. Chem. Soc.* **1995**, *117*, 9026−9032.
(11) Fees, J.; Kaim, W.; Moscherosch, M.; Matheis, W.; Klima, J.; Krejcik, M.; Zalis, S. *Inorg. Chem.* **1993**, *32*, 166−174.
(12) Fees, J.; Ketterle, M.; Klein, A.; Fiedler, J.; Kaim, W. *J. Chem. Soc., Dlat. Trans.* **1999**, *15*, 2595−2600.
(13) Amouyal, E.; Homsi, A.; Chambron, J.-C.; Sauvage, J.-P. *J. Chem. Soc., Dalt. Trans.* **1990**, 1841−1845.
(14) Coates, C. G.; Olofsson, J.; Coletti, M.; McGarvey, J. J.; Oenfelt, B.; Lincoln, P.; Norden, B.; Tuite, E.; Matousek, P.; Parker, A. W. *J. Phys. Chem. B* **2001**, *105*, 12653−12664.
(15) Ujj, L.; Coates, C. G.; Kelly, J. M.; Kruger, P. E.; McGarvey, J. J.; Atkinson, G. H. *J. Phys. Chem. B* **2002**, *106*, 4854−4862.
(16) Onfelt, B.; Lincoln, P.; Norden, B.; Baskin, J. S.; Zewail, A. H. *Proc. Natl. Acad. Sci. U.S.A.* **2000**, *97*, 5708−5713.
(17) Chiorboli, C.; Rodgers, M. A. J.; Scandola, F. *J. Am. Chem. Soc.* **2003**, *125*, 483−491.
(18) Chiorboli, C.; Bignozzi, C.-A.; Scandola, F.; Ishow, E.; Gourdon, A.; Launay, J.-P. *Inorg. Chem.* **1999**, *38*, 2402−2410.
(19) Chiorboli, C.; Fracasso, S.; Scandola, F.; Campagna, S.; Serroni, S.; Konduri, R.; MacDonnell, F. M. *Chem. Comm.* **2003**, 1658−1659.
(20) Chiorboli, C.; Sandro, F.; Ravaglia, M.; Scandola, F.; Campagna, S.; Wouters, K. L.; Konduri, R.; MacDonnell, F. M. *Inorg. Chem.* **2005**, *44*, 8368−8378.
(21) Campagna, S.; Serroni, S.; Bodige, S.; MacDonnell, F. M. *Inorg. Chem.* **1999**, *38*, 692−701.
(22) Bolger, J.; Gourdon, A.; Ishow, E.; Launay, J.-P. *Inorg. Chem.* **1996**, *35*, 2937−2944.
(23) Kim, M.-J.; Konduri, R.; Ye, H.; MacDonnell, F. M.; Puntoriero, F.; Serroni, S.; Campagna, S.; Holder, T.; Kinsel, G.; Rajeshwar, R. *Inorg. Chem.* **2002**, *41*, 2471−2476.
(24) Konduri, R.; de Tacconi, N. R.; Rajeshwar, K.; MacDonnell, F. M. *J. Am. Chem. Soc.* **2004**, *126*, 11621−11629.
(25) Konduri, R.; Ye, H.; MacDonnell, F. M.; Serroni, S.; Campagna, S.; Rajeshwar, K. *Angew. Chem., Int. Ed.* **2002**, *41*, 3185−3187.
(26) de Tacconi, N. R.; Lezna, R. O.; Konduri, R.; Ongeri, F.; Rajeshwar, K.; MacDonnell, F. M. *Chem. Eur. J.* **2005**, *11*, 4327−4339.
(27) Janaratne, T. K.; Yadav, A.; Ongeri, F.; MacDonnell, F. M. *Inorg. Chem.* **2007**, *46*, 3420−3422.
(28) Armaroli, N.; Balzani, V. *Angew. Chem., Int. Ed.* **2007**, *46*, 52−66.
(29) Eisenberg, R.; Nocera, D. G. *Inorg. Chem.* **2005**, *44*, 6779−6781.
(30) Alstrum-Acevedo, J. H.; Brennaman, M. K.; Meyer, T. J. *Inorg. Chem.* **2005**, *44*, 6802−6827.
(31) Dempsey, J. L.; Esswein, A. J.; Manke, D. R.; Rosenthal, J.; Soper, J. D.; Nocera, D. G. *Inorg. Chem.* **2005**, *44*, 6879 -6892.
(32) Balzani, V.; Ceroni, P.; Maestri, M.; Saudan, C.; Vicinelli, V. *Top. Curr. Chem.* **2003**, *228*, 159−191.
(33) Sun, L.; Hammarstrom, L.; Akermark, B.; Styring, S. *Chem. Soc. Rev.* **2001**, *30*, 36−49.
(34) Elvington, M.; Brewer, K. J. *Inorg. Chem.* **2006**, *45*, 5242−5244.
(35) Molnar, S. M.; Nallas, G.; Bridgewater, J. S.; Brewer, K. J. *J. Am. Chem. Soc.* **1994**, *116*, 5206−5210.
(36) Rosenthal, J.; Bachman, J.; Dempsey, J. L.; Esswein, A. J.; Gray, T. G.; Hodgkiss, J. M.; Manke, D. R.; Luckett, T. D.; Pistorio, B. J.; Veige, A. S.; Nocera, D. G. *Coord. Chem. Rev.* **2005**, *249*, 1316−1326.
(37) Heyduk, A. F.; Nocera, D. G. *Science* **2001**, *293*, 1639−1641.
(38) Esswein, A. J.; Veige, A. S.; Nocera, D. G. *J. Am. Chem. Soc.* **2005**, *127*, 16641−16651.
(39) Pfennig, B. W.; Mordas, C. J.; McCloskey, A.; Lockard, J. V.; Salmon, P. M.; Cohen, J. L.; Watson, D. F.; Bocarsly, A. B. *Inorg. Chem.* **2002**, *41*, 4389−4395.
(40) Chang, C. C.; Pfennig, B.; Bocarsly, A. B. *Coord. Chem. Rev.* **2000**, *2008*, 33−45.
(41) Borgstrom, M.; Shaikh, N.; Johansson, O.; Anderlund, M. F.; Styring, S.; Akermark, B.; Magnuson, A.; L., H. *J. Am. Chem. Soc.* **2005**, *127*, 17504−17515.
(42) Wärnmark, K.; Thomas, J. A.; Heyke, O.; Lehn, J.-M. *Chem. Commun.* **1996**, 701−702.
(43) Szwarc, M.; Jagur-Grodzinski, J. *Ions Ion Pairs Org. React.* **1974**, *2*, 1−150.
(44) Staples, T. L.; Jagur-Grodzinski, J.; Szwarc, M. *J. Am. Chem. Soc.* **1969**, *91*, 3721−3723.
(45) Hay, R. S.; Pomery, P. J. *Austr. J. Chem.* **1971**, *24*, 2287−2292.
(46) Barradas, R. G.; Gust, S. L.; Porter, J. D. *Tetrahedron Lett.* **1981**, *22*, 4579−4582.
(47) Cserhegyi, A.; Jagur-Grodzinski, J.; Szwarc, M. *J. Am. Chem. Soc.* **1969**, *91*, 1892−1895.
(48) Chaudhuri, J.; Kume, S.; Jagur-Grodzinski, J.; Szwarc, M. *J. Am. Chem. Soc.* **1968**, *90*, 6421−6425.
(49) Bolger, J.; Gourdon, A.; Ishow, E.; Launay, J.-P. *J. Chem. Soc., Chem. Comm.* **1995**, *17*, 1799−1800.
(50) Tokel-Takvoryan, N. E.; Hemingway, R. E.; Bard, A. J. *J. Am. Chem. Soc.* **1973**, *95*, 6582.
(51) Goss, C. A.; Abruña, H. D. *Inorg. Chem.* **1985**, *24*, 4263−4267.
(52) Bernhard, S.; K., T.; Diaz, D. J.; Abruña, H. D.; H., M. *J. Am. Chem. Soc.* **2001**, *123*, 10265−10271.
(53) Bilakhiya, A. K.; Tyagi, B.; Paul, P.; Natarajan, P. *Inorg. Chem.* **2002**, *41*, 3830−3842.
(54) Ishow, E.; Gourdon, A.; Launay, J.-P. *Chem. Comm.* **1998**, 1909−1910.
(55) Ishow, E.; Gourdon, A.; Launay, J.-P.; Chiorboli, C.; Scandola, F. *Inorg. Chem.* **1999**, *38*, 1504−1510.
(56) Bergman, S. D.; Kol, M. *Inorg. Chem.* **2005**, *44*, 1647−1654.
(57) Elias, B.; Herman, L.; Moucheron, C.; Kirsch-De Mesmaeker, A. *Inorg. Chem.* **2005**, *44*, 7678−7685.
(58) Steullet, V.; Dixon, D. W. *J. Chem. Soc., Perkin Trans. 2* **1999**, 1547−1558.
(59) Gut, D.; Golberg, I.; Kol, M. *Inorg. Chem.* **2003**, *42*, 3483−3491.
(60) Bergman, S. D.; Golberg, I.; Barbieri, A.; Barigelleti, F.; Kol, M. *Inorg. Chem.* **2004**, *43*, 2355−2367.
(61) Giraudeau, A.; Louati, A.; Gross, M.; Andre, J. J.; Simon, J.; Su, C. H.; Kadish, K. M. *J. Am. Chem. Soc.* **1983**, *105*, 2917−2919.
(62) Kadish, K. M.; Sazou, D.; Liu, Y. M.; Saoiabi, A.; Ferhat, M.; Guilard, R. *Inorg. Chem.* **1998**, *27*, 686−690.
(63) Ruiz, G. T.; Juliarena, M. P.; Lezna, R. O.; Feliz, M. R.; Ferraudi, G. *J. Photochem Photobio. A* **2006**, *179*, 289−297.
(64) Juliarena, M. P.; Lezna, R. O.; Feliz, M. R.; Ruiz, G. T.; Thomas, S.; Ferraudi, G.; Carmichael, I. *J. Org. Chem.* **2006**, *71*, 2870−2873.
(65) Kadish, K. M.; Sazou, D.; Liu, Y. M.; Saoiabi, A.; Ferhat, M.; Guilard, R. *Inorg. Chem.* **1988**, *27*, 686−690.
(66) Rapta, P.; Schulte, N.; Schlüter, A. D.; Dunsch, L. *Chem. Eur. J.* **2006**, *12*, 3103−3113.
(67) Lü, J.-M.; Rosokha, S. V.; Kochi, J. K. *J. Am. Chem. Soc.* **2003**, *125*, 12161−12171.
(68) Ganesan, V.; Rosokha, S. V.; Kochi, J. K. *J. Am. Chem. Soc.* **2003**, *125*, 2559−2571.
(69) Vazquez, C.; Calabrese, J. C.; Dixon, D. A.; Miller, J. S. *J. Org. Chem.* **1993**, *58*, 65−81.

(70) Johnson, M. T.; Arif, A. M.; Miller, J. S. *Eur. J. Inorg. Chem.* **2000**, 1781−1787.
(71) Novoa, J. J.; Lafuente, P.; Del, Sesto, R. E.; Miller, J. S. *Cryst. Eng. Comm.* **2002**, *4*, 373−377.
(72) Awere, E. G.; Burford, N.; Haddon, R. C.; S., P.; Passmore, J.; Waszczak, J. V.; White, P. S. *Inorg. Chem.* **1990**, *29*, 4821−4830.
(73) Gundel, D.; Sixl, H.; Metzger, R. M.; Heimer, N. E.; Harms, R. H.; Keller, H. J.; Nothe, D.; Wehe, D. *J. Chem. Phys.* **1983**, *79*, 3678−3688.
(74) Grossel, M. C.; Weston, S. C. *Chem. Mater.* **1996**, *8*, 977−980.
(75) Novoa, J. J.; Lafuente, P.; Del, Sesto, R. E.; Miller, J. S. *Angew. Chem., Int. Ed. Engl.* **2001**, *40*, 2540−2545.
(76) Yu, Y.; Gunic, E.; Zinger, B.; Miller, L. L. *J. Am. Chem. Soc.* **1996**, *118*, 1013−1018.
(77) Levillain, E.; Roncali, J. *J. Am. Chem. Soc.* **1999**, *121*, 8760−8765.
(78) Zheng, S.; Lan, J.; Khan, S. I.; Rubin, Y. *J. Am. Chem. Soc.* **2003**, *125*, 5786−5791.